Thin Solid Films 627 (2017) 82–93

Contents lists available at ScienceDirect

Thin Solid Films

journal homepage: www.elsevier.com/locate/tsf

Preparation and characterization of poly (3-hexylthiophene) sensitized Ag doped TiO_2 nanotubes and its carrier density under solar light illumination

Evrim Baran [a,*], Birgül Yazıcı [b]

[a] Department of Chemistry, Kilis 7 Aralık University, Faculty of Science and Literature, Kilis 79000, Turkey
[b] Department of Chemistry, Çukurova University, Science and Letters Faculty, Adana 01330, Turkey

ARTICLE INFO

Article history:
Received 21 June 2016
Received in revised form 20 February 2017
Accepted 22 February 2017
Available online 27 February 2017

Keywords:
Poly (3-hexylthiophene)
Silver-doped titania-nanotubes
Scanning electron microscopy
X-ray diffraction
Electrochemical impedance spectroscopy
Mott-Schottky analysis
Solar illumination

ABSTRACT

Poly (3-hexylthiophene) sensitized Ag doped TiO_2-NTs (P3HT/Ag-TiO_2-NTs) have been prepared using the three sequential steps: two step anodization, galvanostatic deposition and spin coating techniques. The morphology and structure of P3HT synthesized by oxidative polymerization with $FeCl_3$ were characterized using NMR, FT-IR, SEM, XRD and optical properties of P3HT were investigated using Uv–Vis technique. The characterization results showed that the P3HT has 64.7%HT-HT configuration, mainly edge-on oriented lamellar structure and the optical band gap of 2.24 eV. Also, the morphology and structure characterization of P3HT/Ag-TiO_2-NTs were determined by FE-SEM and XRD. The electrochemical behaviors of P3HT/Ag-TiO_2-NTs in acetonitrile electrolyte contained I^-/I_3^- were examined by utilizing Electrochemical Impedance Spectroscopy (EIS) and Cyclic Voltammetry (CV). The EIS results displayed that after the modification with P3HT, the value of charge transfer resistance at −0.4 V decreases from 514 Ω cm^2 to 121 Ω cm^2, compared to Ag-TiO_2-NTs. Furthermore, the analysis results of EIS and Mott-Schottky for P3HT/Ag-TiO_2-NTs under simulated solar light revealed that the charge transfer resistance decreased from 121 Ω cm^2 to 51.60 Ω cm^2 and the carrier density (N_D) increased from 8.69×10^{21} cm^{-3} to 70.1×10^{21} cm^{-3}, compared to the values under the absence of solar light. These indicate that P3HT supplies better photogenerated electron-hole pairs separation and mobility.

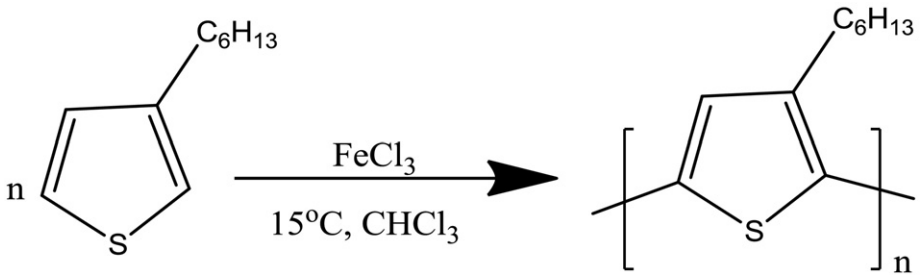
© 2017 Elsevier B.V. All rights reserved.

1. Introduction

The π-conjugated polymers, such as polyaniline, polypyrrole, polythiophene and their derivatives, have attracted considerable attention in the electronic applications, such as solar cells, thin film transistors and light-emitting diodes, due to their interesting photo-physical properties [1,2]. The conjugated polymers having the advantages, containing low cost, ease of fabrication, flexibility and potential of large area production, possess a promising role in the especially application of organic solar cells [3]. Among the conjugated polymers, the poly (3-hexylthiophene) which can easily undergo p-doping when exposed to air or moisture [4] is the most frequently used as a donor materials in the organic solar cell due to the chemical stability, the high crystallinity, the high conductivity and the electronic band gap generally fulling within the visible region, combined with a high hole mobility [5,6]. However, organic solar cells occurred the electron accepting network formed randomly within the polymer matrix suffer from the charge carrier recombination during the charge transport [7–8]. Hence, among the proposed solar cell, the organic-inorganic hybrid solar cells, based on conjugated polymers combined with n-type inorganic semiconductors, have come forward because of potential advantageous properties of both organic polymer and inorganic semiconductor [9]. In the organic-inorganic hybrid solar cells, the conjugated polymers and inorganic semiconductors act as the electron donating light absorbing polymer and the electron acceptor, respectively. These systems supply a large interface area where excitons, bound electron–hole pairs, can effectively dissociate and two separate channels for efficient electron and hole transport [10]. Different inorganic materials including TiO_2 [11], ZnO [12], PbS [13] or CdSe [14], owing to high electron mobility, high dielectric constant and facile control of the size and the shape of nanostructure have been widely used in the organic-inorganic hybrid solar cells. Among them, TiO_2 have attracted considerable interest because of their low cost, non-toxic, high refractive index, good electron acceptable and transportable characteristics and excellent optical transmittance in the visible and near-IR region [7,15]. Additionally, many different nanostructure morphologies of TiO_2 can be synthesis using the methods such as sol-gel [16], hydrothermal [17], anodic oxidation [18]. The nanoparticle [19], nanorod [20], nanotube [21] morphologies of TiO_2 have been popularly used in hybrid solar cells. The TiO_2 nanostructures in designing efficient and stable organic optoelectronic devices such as dye-sensitized solar cells (DSSCs) show significant power conversion

* Corresponding author.
E-mail address: evrimbaran@kilis.edu.tr (E. Baran).

http://dx.doi.org/10.1016/j.tsf.2017.02.051
0040-6090/© 2017 Elsevier B.V. All rights reserved.



Scheme 1. Preparation of P3HT by oxidative polymerization.

efficiency due to the high the specific surface area for the loading of dye molecules [22]. However, the disordered stacking of TiO_2 nanocrystalline limits the electron transport and reduces the electron lifetime because of the random network of misaligned crystallites. Hence, one-dimensional (1D) nanostructures such as nanotubes have been studied as photoanode materials for DSSCs [23]. These TiO_2 nanostructure arrays provide direct pathways for charge transport, dramatically reducing the charge recombination, and large specific surface areas as well as facilitate the coating of more polymeric materials. The properties such as efficient generation of photo-excited electrons and good light-scattering possessed by TiO_2 nanostructure play important roles in obtaining high efficiency DSSC [24].

In the organic solar cells, it has been reported that the addition of metal nanoparticles into the semiconductors can increase the light absorption in the visible region, leading to enhancement in the performance of solar cell by creating additional energy levels within the band gap of these semiconductors [25]. Additionally, as the incorporation of metal nanoparticles interacts with the light having wavelength much larger than the size of particle, it creates collective oscillations of valence electrons known as surface plasmon resonance and enhance light absorption and photocurrent generation in the organic solar cell [26,27]. The Ag and Au nanoparticles which are suitable to support surface plasmonic propagation and resonance are extensively used to enhance of photovoltaic conversion efficiency from organic solar cells [28]. It was reported in the literature that >45% enhancement in the photocurrent was achieved using AgNPs in TiO_2 film sensitized with carbazole based dye [29].

In this paper, we report on the fabrication and characterization of poly (3-Hexylthiophene) Sensitized Ag Doped TiO_2-NTs. The characterizations of the synthesized P3HT were examined in detail using proton Nuclear magnetic resonance spectroscopy (^{1}H NMR), Fourier transform infrared spectra (FT-IR), X-ray diffraction (XRD), UV–visible spectra and field emission-scanning electron microscope (FE-SEM). The P3HT film was prepared on Ag-TiO_2-NTs by spin coating technique. The effect of

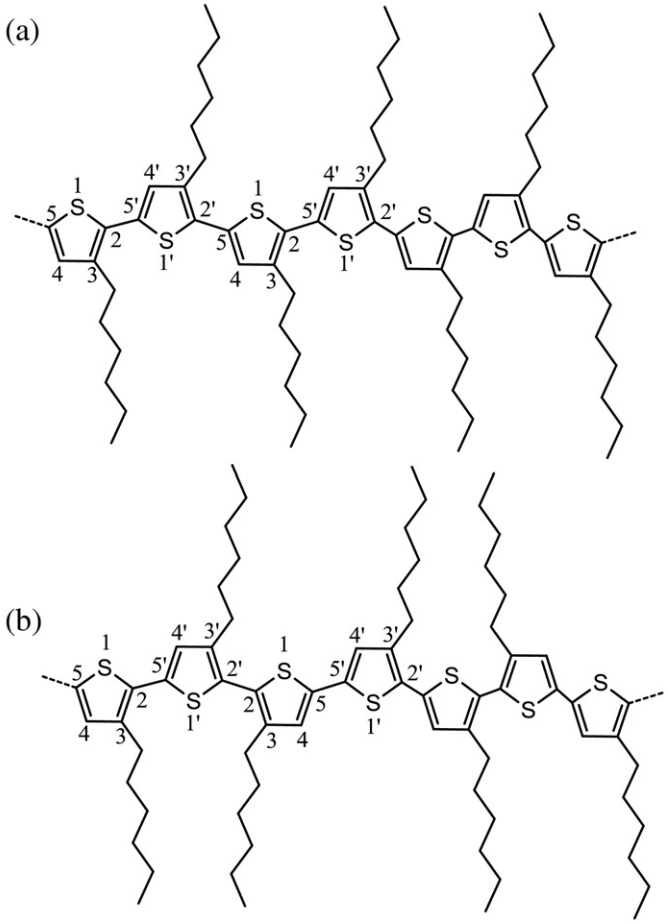


Fig. 1. (a) Regioregular and (b) regioirregular of P3HT.

the interface modification on the performance of charge transport was investigated by electrochemical impedance spectroscopy (EIS) and Mott–Schottky analysis. Additionally, under simulated solar light, electronic parameters (flat band potential, carrier density) of the P3HT/Ag-TiO_2-NTs were determined.

2. Materials and methods

2.1. Materials

Ammonium fluoride (NH_4F), anhydrous $FeCl_3$, ethylene glycol (99.5%), hydrofluoric acid (HF, 38%), nitric acid (HNO_3, 65%), LiI (99.9%), I_2 (99.8%), 4-tert-butylpyridine (96%), acetone, 2-prapanol, tetrahydrofuran and methanol were purchased from Merck company. Silver nitrate ($AgNO_3$), 3-hexylthiophene (3HT) and titanium foils with thickness of 0.25 mm (99.7% purity) were received from Sigma-Aldrich. All the chemical reagents were analytical grade without further purification. All experiments were carried out at room temperature using distillated water.

2.2. Synthesis of TiO_2-NTs and Ag doped TiO_2-NTs electrodes

Prior to the synthesis of TiO_2-NTs, the Ti foils with size of 1.5 × 1 cm were chemically polished in a mixture of HF (4 wt%) and HNO_3 (6.5 wt%) (1:3 in volume) for 10 s, followed by mechanically polished and degreased by ultrasonic cleaning in acetone, isopropanol, methanol and distilled water for 10 min, respectively. Then the foils were dried in the oxygen stream. TiO_2-NTs electrodes were synthesis by a two-step anodization technique. All anodization experiments were carried out using a direct current (DC) voltage source (AA TECH APS-3303DD). Ti foils were used as anodic electrode while platinum (10 × 10 × 0.1 mm) was used as cathodic electrode. The ethylene glycol solution containing 0.3 wt% of NH_4F and 2 wt% of H_2O was used as anodization bath. In the first-step anodization, the Ti foils were anodized at 60 V for 2 h and the as-grown nanotube layers were ultrasonically removed in distilled water. The second anodization was carried out on the same Ti foils at 21 V for 4 h. After anodization, the samples were washed in distilled water and dried in air. TiO_2-NTs electrodes were annealed at 450 °C for 1 h in atmosphere. Ag particles were deposited on the TiO_2-NTs by the galvanostatic method using a three-electrode system with the TiO_2-NTs as the working electrode, a Pt counter electrode and Ag/AgCl (3 M KCl) reference electrode. The galvanostatic deposition was carried out at 0.3 mA for 240 s in aqueous solution containing 0.75 mM $AgNO_3$. After electrodeposition process, Ag-TiO_2-NTs electrodes were washed with distilled water and then dried in the air at 80 °C.

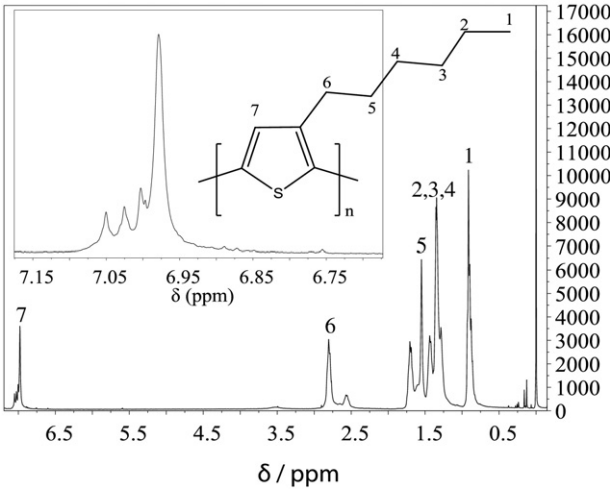


Fig. 2. ^{1}HNMR spectrum of P3HT.

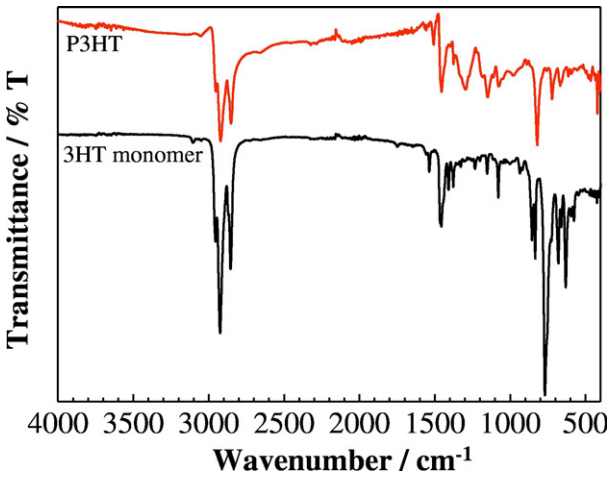


Fig. 3. FT-IR spectra of 3HT monomer and P3HT prepared by chemical oxidative polymerization.

2.3. Synthesis of P3HT

The poly(3-hexylthiophene) (P3HT) was synthesized by common oxidative polymerization method at 15 °C using anhydrous $FeCl_3$ as a catalyst in chloroform under nitrogen atmosphere (Scheme 1). 1.3 g (7.73 × 10^{-3} mol) of 3-hexylthiophene (3HT)

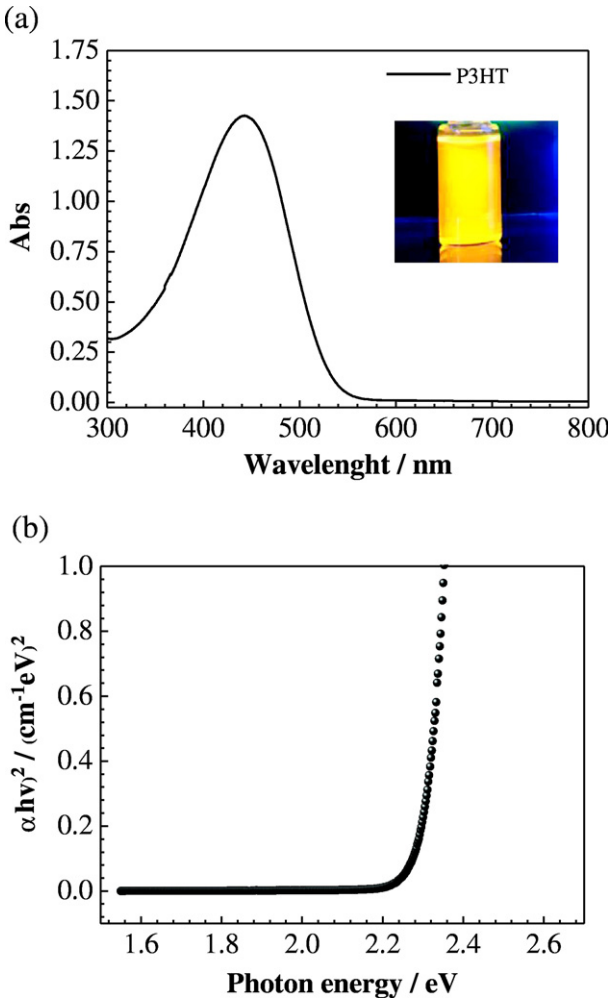


Fig. 4. (a) UV–vis spectra of 3HT monomer and P3HT and (b) Tauc plots for the determination of optical band gap for P3HT.

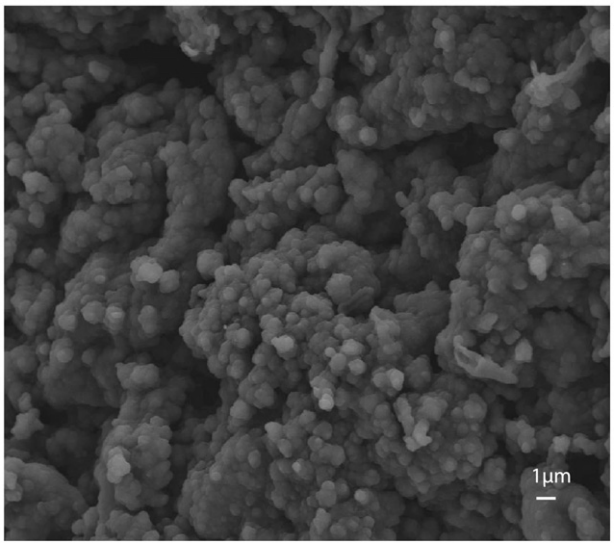


Fig. 5. The SEM image of P3HT powder.

dissolved in 20 ml of $CHCl_3$ was added to 3.77 g (2.30×10^{-2} mol) of anhydrous $FeCl_3$ dissolved in 100 ml of $CHCl_3$. The reaction mixture was allowed to stir at 15 °C for 12 h and then was poured into large amount of methanol. The precipitate obtained was filtered and washed with methanol, HCl (10 vol%), acetone, NH_4OH (10 vol%), ethylenediaminetetraacetic acid (EDTA 1%) and distilled water. The product was then dried, yielding a dark brown P3HT (0.8213 g).

2.4. Preparation of P3HT/Ag-TiO_2 nanocomposite

The P3HT was dissolved in tetrahydrofuran (THF) at a concentration of 10 mg/ml. The mixture was stirred for 30 min and then the insoluble material was removed by centrifugation. The solution was evaporated until the volume of solution is half. The P3HT solution was spin coated twice on the Ag-TiO_2-NTs at 3000 rpm for 15 s and the residual solvent was removed by drying the samples in a vacuum oven at 65 °C for 24 h.

2.5. Characterization

The FT-IR spectrum of the synthesized P3HT was recorded within the wavelength range between 4000 and 400 cm^{-1} using a FT-IR spectrometer (Thermoscientific Nicolet iS10). The ^1H NMR spectrum of the P3HT was recorded on a Bruker 400 Avance III spectrometer (^1H: 400 MHz). Chloroform-*d*, $CDCl_3$, was used as solvent, and tetramethylsilane (TMS) was used the internal standard for NMR analyses. UV–visible absorption spectrum of the chloroform solution of P3HT was recorded on a PG Instrument T80 + UV–vis spectrophotometer. The morphologies of TiO_2-NTs, Ag-TiO_2-NTs and P3HT/Ag-TiO_2 electrodes were examined by field emission scanning electron microscope (FE-SEM, Zeiss/Supra 55 SEM at high vacuum and 10.00 kV EHT). Crystal structures of the P3HT and electrodes were determined by X-ray diffraction (XRD) using Rigaku Smart Lab diffractometer, with Cu Kα radiation operated at 40 kV and 30 mA. The scattered intensity was scanned in the 2θ range 3–90° with a scan rate of 3° min^{-1}.

2.6. Electrochemical measurement

The electrochemical measurements were carried out in acetonitrile electrolyte contained 0.5 M LiI, 0.05 M I_2 and 0.5 M 4-tert-

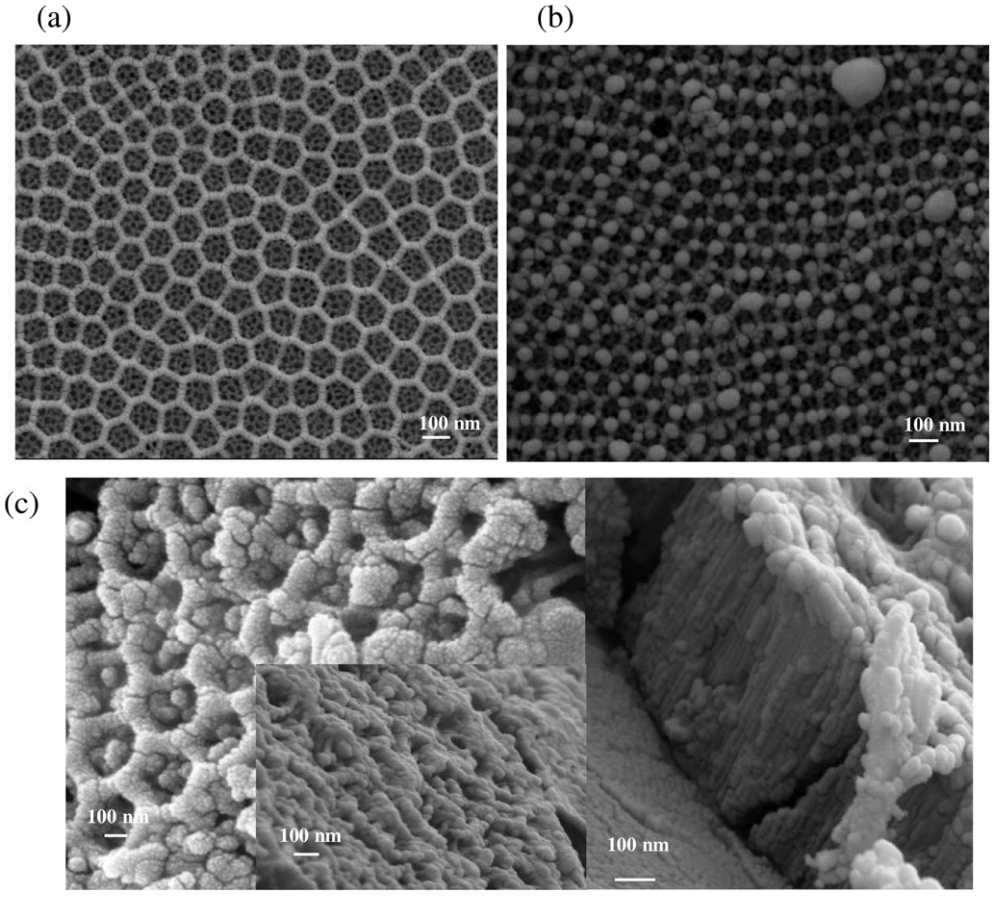


Fig. 6. FE-SEM images of (a) TiO_2-NTs, (b) Ag-TiO_2-NTs and (c) P3HT/Ag-TiO_2-NTs electrodes.

butylpyridine with a standard three-electrode cell composed of the obtained sample, platinum sheet (with 2 cm^2 surface area) and Ag/AgCl (3 M KCl) as the working, counter and reference electrode, respectively, using a CHI 604E A.C. electrochemical analyzer at room temperature, open to atmosphere. The electrochemical measurements were also recorded under 100 mW cm^{-2} simulated AM 1.5 G solar light irradiation (Abet Solar Simulator Sun2000). The cyclic voltammetry measurements were obtained in the potential ranges between −0.6 V and 1.8 V with a scan rate of 0.1 V s^{-1}. Current-voltage curves were obtained from −0.2 V to 1.8 V (Ag/AgCl) at a sweep rate of 0.01 V s^{-1} after 1 h of electrode immersion in acetonitrile electrolyte contained I^-/I_3^- under solar light irradiation. Open circuit voltage-time curves of P3HT/Ag-TiO_2-NTs electrodes were recorded during continuous illumination of 1 h and under absence of solar light in ambient conditions in acetonitrile electrolyte contained I^-/I_3^-. In presented work, the Mott-Schottky approach was used to determine differences in the electronic properties of the obtained sample. For this purpose, the EIS experiments were conducted in the frequency range of 100 kHz–0.1 Hz, with the amplitude voltage of 5 mV, under different applied potentials in the range −1.2 V to 1.2 V with 0.2 V steps. The EIS results were analyzed using the Zview software.

3. Results and discussion

3.1. Characterization and optical properties of P3HT

3-Hexylthiophene, being an asymmetric monomer, causes different regioisomers during the polymerization when the monomers are coupled through the 2- and 5-positions: head to head coupling (HH, 2-2′), head to tail coupling (HT, 2-5′), and tail to tail coupling (TT, 5-5′) [30]. Thus, P3HT exhibits a different regiochemistry as shown in Fig. 1. P3HT containing only HT couplings are referred to as regioregular, while the polymer containing a mixture of HH and TT couplings are referred to as regioirregular [31]. The regioirregular structure having an unfavorable HH conformation gives rise to a decrease in the conjugation length. In contrast, the regioregular structure of P3HT displays a lower π-π* transition with extended π-conjugation [31]. To confirm the polymerization of 3HT and determined the percentages of its regioisomers, the ^1H NMR analysis was carried out. Fig. 2 shows the ^1H NMR of P3HT in $CDCl_3$. The ^1H NMR spectra of P3HT demonstrates the main signals: 6.98 ppm (thiophene H7 position); 2.80–2.57 ppm (—CH_2 to the thiophene ring (H6 position)); 1.55 ppm (—CH_2, H5 position); 1.35–1.29 ppm (other methylene, H2–4 positions); 0.91 ppm (—CH_3, H1 position). The results were found to be in agreement with the chemical shift data reported in the previous studies [32–34]. The relative abundance of HT, HH and TT configurations described the regiochemistry of P3HT can be determined via ^1H NMR spectroscopy by integration of the peaks corresponding to the methylene group α to the thiophene ring ($\delta = 2.57$ ppm ascribed to HH configuration and 2.80 ppm ascribed to HT configuration) or in the aromatic region of the ^1H NMR spectrum ($\delta = 6.98$ ppm (HT-HT), 7.00 ppm (HT-HH), 7.03 ppm (TT-HT) and 7.05 ppm (HH-TT)) [35]. When using the signals at 2.57–2.80 ppm, the relative ratio of HT:HH dyads in the P3HT was estimated as 77:23. Alternatively, on the basis of the signals in the aromatic region, the percentages of the HT-HT, HT-HH, TT-HT, and TT-HH triads were found to be 64.7%, 14.5%, 11.4% and 9.4%, respectively. The characterization results of the synthesized P3HT indicated that P3HT consists of 64.7% regioregular (HT-HT) and 35.7% regioirregular (HT-HH, TT-HT, and TT-HH) configurations. The degree of regioregularity has a large effect on the electrical and optical properties of P3HT and increasing the content of HH and TT dyads results in increased steric repulsion and reduces the inter-annular pi orbital overlap (the effective conjugation length) [36]. Therefore, it is important to determine the rate of regioregular for their use in technological applications requiring the conductive form of the conjugated polymer.

The FT-IR spectra of 3HT monomer and P3HT are shown in Fig. 3. In the FT-IR spectra of P3HT, the peaks at 2952, 2921 and 2852 cm^{-1} are assigned to the CH_3 asymmetric stretching vibrations, CH_2 in-phase stretching and the CH_2 out-of-phase stretching in the aliphatic group, respectively [37]. The band at 1507 and 1455 cm^{-1} are attributed to the antisymmetric C═C stretching and symmetric stretching in the thiophene ring, respectively [38]. The intensity ratio of the peaks

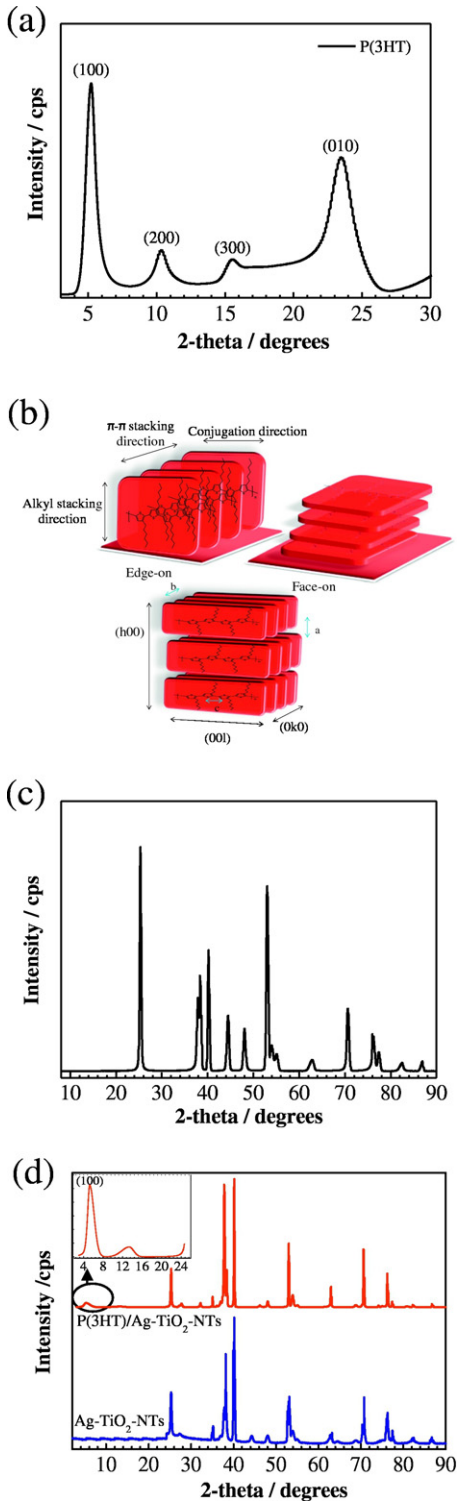


Fig. 7. (a) XRD patterns of P3HT powder, (b) two typical P3HT chain orientations, edge-on and face-on, where the lattice constants a, b, c are the distance between backbones, stacking distance, and distance between side chains, respectively, XRD patterns of (c) TiO_2-NTs, (d) Ag-TiO_2-NTs and P3HT/Ag-TiO_2-NTs electrodes, respectively.

corresponding to the asymmetric C=C stretching (I_{1507}) and the symmetric stretching (I_{1455}) is indicative of conjugation length [6]. The intensity ratio (I_{1507}/I_{1455}) of the synthesized P3HT was calculated to be 0.64. The bands at 1296 and 1149 cm^{-1} are associated with C—H bending [10,39]. The peaks around 820 and 722 cm^{-1} represent the C—H out-of-plane and CH_3 rocking vibrations, respectively [6]. Additionally, the band at 820 cm^{-1} is an indication of 2,5 linked P3HT [2]. The Uv–Vis spectrum of the P3HT in chloroform solution is shown in Fig. 4a. The maximum absorption of P3HT was observed at 442 nm, consistent with the literature [40,41]. The band at 442 nm corresponds to the π-π* transition of the conjugated chain in the P3HT polymer [38]. A prediction of Fermi level differences between the regioirregular and regioregular P3HT structures can be carried out by observing the band edge of the spectra [42]. The band gap for regioregular P3HT has been reported to range from 1.8 to 1.9 eV, the 2.2 eV informed for regioirregular P3HT in the literature [43,44]. The optical band gap (E_g) of P3HT consisted of 64.7% HT-HT configuration, estimated using Tauc's approach $(\alpha h\nu)^2 = A(h\nu - E_g)$, was determined to be 2.24 eV (Fig. 4b). The surface morphology of the synthesized P3HT powder was analyzed by FE-SEM and the FE-SEM image is presented in Fig. 5. The image exhibits that the P3HT powder possesses particles of 300–900 nm with irregular morphology due to the agglomeration of the particles.

3.2. Structural and morphological analysis of P3HT/Ag-TiO_2 nanocomposite

The SEM image of TiO_2-NTs synthesized on the surface of Ti foil is shown in Fig. 6a. The inner diameters of the obtained nanotube were determined to be about 35 nm and the pore diameters of honeycomb lattice on the surface of TiO_2-NTs were found to be approximately 175 nm. The morphology of Ag doped TiO_2-NTs electrode obtained at 0.3 mA after 240 s of electrochemical deposition is illustrated in Fig. 6b. As seen from Fig. 6b, after 240 s of galvanostatic deposition, the Ag nanoparticles (NPs), having a size in the range of 48–90 nm, could be deposition on the top, inside and outside surface of honeycomb lattice covered TiO_2-NTs. The SEM images of P3HT/Ag-TiO_2 nanocomposite are presented in Fig. 6c. After spin coating of P3HT, the top surface of Ag-TiO_2-NTs was exactly covered by P3HT. The cross-section view as shown in Fig. 6c, indicates that the ends of Ag-TiO_2-NTs were closed by P3HT and the gaps between nanotubes were filled by the P3HT.

The XRD pattern of the synthesized P3HT in Fig. 7a exhibits four distinct peaks at 2θ = 5.21°, 10.32°, 15.49° and 23.44°, corresponding to out of plane diffraction patterns for the (100), (200), (300) and (010) peaks, respectively [45]. The presence of peaks at 2θ = 5.21°and 23.44° indicates that the P3HT sample has mainly edge-on oriented lamella layer structure with a minority of face-on lamella (Fig. 7b). The result represents that the chains of P3HT are primarily parallel to the substrate and minor fraction of chains are face-on oriented [46]. The d-spacing values corresponding to the peaks at 2θ = 5.21° and 23.44°, which represent the intrachain distance between P3HT chains and the stacking distance of the thiophene rings or interplanar distance, respectively, were determined to be 16.95 Å and 3.79 Å, which consistent with the results presented in the literature [37,47–49]. As seen in Fig. 7c, the XRD pattern of Ag-TiO_2-NTs displays that the diffraction peaks observed at 2θ = 25.2°, 38.2°, 48.0°, 53.9°, and 62.8° are associated with the crystalline planes (101), (004), (200), (105) and (204) of tetragonal structured anatase TiO_2, and at 2θ values of 37.9°, 44.2°, 64.5°, 77.6° and 81.7° corresponding to (111), (200), (220), (311) and (222) planes of face centered cubic structured Ag metal [50]. Fig. 7c also shows the XRD patterns for P3HT/Ag-TiO_2 nanocomposite. All observed peaks in the XRD of P3HT/Ag-TiO_2 are consistent with the diffraction peaks of anatase TiO_2 and cubic Ag and the peak at 5.22° corresponding to the strong (100) plane of P3HT was also detected. The strong peak at 5.22° indicates that the P3HT chain in the P3HT/Ag-TiO_2 nanocomposite film have a tendency to orient parallel to the Ag-TiO_2-NT surface. Also, the intrachain distances $d_{[100]}$ of the P3HT packing for the pure P3HT and the P3HT/Ag-TiO_2 nanocomposite were found to be 16.95 Å and 16.90 Å, respectively.

The average particle sizes were estimated using the Scherrer equation for the (101) diffraction plane of anatase TiO_2, (111) diffraction plane of Ag and (100) diffraction plane of P3HT [41]:

$$D = \frac{k\lambda}{\beta \cos\theta} \tag{1}$$

where D is the crystal size, k is the constant (0.89), λ is the X-ray wavelength (1.54 Å), β is the full width at half maximum (FWHM) of the TiO_2, Ag and P3HT peaks, θ is the diffraction angle.

For anatase TiO_2 and Ag, the lattice constants and volume of the unit cell (V) are calculated using the following formula [51,52].

For anatase TiO_2:

$$\frac{1}{d^2} = \frac{h^2 + k^2}{a^2} + \frac{l^2}{c^2} \tag{2}$$

$$V = a^2 \times c \tag{3}$$

For cubic silver:

$$\frac{1}{d^2} = \frac{h^2 + k^2 + l^2}{a^2} \tag{4}$$

$$V = a^3 \tag{5}$$

where (hkl) and d are the Miller indices of lattice planes and inter planar spacing of lattice planes, respectively. The lattice parameters and the crystal sizes calculated for anatase TiO_2-NTs, cubic Ag and P3HT are listed in Table 1. The calculated values of lattice parameter were found to be consistent with standard ones. It is seen from Table 1 that the anatase TiO_2 have crystallite size of 22.43 nm and after the doping of Ag, the crystallite size of TiO_2-NTs was decreased to 16.59 nm. When the P3HT was coated on the surface of Ag-TiO_2-NTs, the crystallite size value further increased to 34.36 nm. These results can be explained that introduction of Ag causing shrinkage of some of the TiO_2 crystallite planes, resulting in disordering of crystallinity of the TiO_2 and the coating of P3HT may lead to increased numbers of point defects, which would give rise to higher grain boundary mobility and grain growth

Table 1
Structural parameters of TiO_2-NTs, Ag-TiO_2-NTs, P3HT/Ag-TiO_2-NTs electrodes and P3HT powder calculated from the XRD results.

	Anatase TiO_2-NTs[a]				Ag nanoparticles[b]			P3HT
	Lattice constants (Å)		D (nm)	V (Å^3)	Lattice constants (Å)	D (nm)	V (Å^3)	D (nm)
	a	c			a			
TiO_2-NTs	3.788	9.507	22.43	136.43	–	–	–	–
Ag-TiO_2-NTs	3.799	9.428	16.59	136.06	4.082	24.73	68.04	–
P3HT	–	–	–	–	–	–	–	9.60
P3HT/Ag-TiO_2-NTs	3.786	9.526	34.36	136.56	4.079	15.57	67.91	5.17

[a] Standard values a = b = 3.783 Å and c = 9.510 Å for anatase TiO_2 (JCPDS Card no 04-0477).
[b] Standard values a = b = c = 4.079 (JCPDS Card no 01-1164).

rates [53]. The lattice parameters 'a' and 'c' values of TiO_2-NTs were calculated to be 3.788 Å and 9.507 Å, respectively. When the lattice parameters of TiO_2 examined in the Table 1, a change takes place only in c-axis, while 'a' lattice parameter remains almost constant. This may be explained that to balance this compressive internal stress caused by incorporation of foreign atoms or ions in place of Ti^{+4} lattice sites, c lattice expansion in vertical direction [54]. The pure P3HT crystallite size was found to be 9.60 nm, whereas the crystallite size after the coating of P3HT on the surface of Ag-TiO_2-NTs was calculated to be 5.17 nm. The observed decrease of the P3HT crystallite size is associated with the disordering of the polymer chains [55].

3.3. Electrochemical characterization

In order to explain the influence of the P3HT coated on the surface of Ag-TiO_2-NTs electrode on the charge transport at the electrode/electrolyte interface, the measurements of electrochemical impedance spectroscopy (EIS) was performed at various potentials. All the EIS results were fitted using the equivalent circuit models in the inset of Fig. 8. In the suggested equivalent circuit, R_s represents resistance of the I^-/I_3^- solution, R_1/CPE_1 couple are attributed to the resistance of the charge transfer ($I_3^- + 2e^-_{cb\ (TiO2\text{-}NTs)} = 3I^-$) and the double layer capacitance occurred at the interface between of P3HT/Ag-TiO_2-NTs (or Ag-TiO_2-NTs or TiO_2-NTs for the other electrodes) film and the bulk electrolyte. On the other side, R_2 and CPE_2 are the resistance and the capacitance of compact TiO_2 layer. EIS data (Nyquist, bode and phase angle plots) obtained at −0.4 V for P3HT/Ag-TiO_2-NTs, Ag-TiO_2-NTs and TiO_2-NTs electrodes are presented in Fig. 8. The charge transfer resistances (R_1) of TiO_2-NTs, Ag-TiO_2-NTs and P3HT/Ag-TiO_2-NTs electrodes are 574 Ω cm^2, 514 Ω cm^2 and 121 Ω cm^2, respectively. The P3HT/Ag-TiO_2-NTs electrode has the lowest value among the three kind's electrodes. The lower charge transfer resistance could provide a more rapid and effective charge transfer at the interface and that the photoexcited electrons have enough time to reach the electrode before the recombination takes place [56,57]. CPE consists of two parameters, namely admittance magnitude (Y) and exponent (n) [58]. Due to the Y value of CPE parameter cannot represent the capacitance when $n < 1$ [59]. C_{eff} is a parameter that keeps any non-ideal capacitive characteristics of the R/CPE system. The effective capacitance (C_{eff}) was calculated from the following equation [60]:

$$C_{eff} = Y^{1/n} R^{(1-n)/n} \quad (6)$$

The electrochemical double layer capacitance is increased from 289.81 μF cm^{-2} (TiO_2-NTs) to 421.01 μF cm^{-2} (P3HT/Ag-TiO_2-NTs). The increase in capacitance is consistent with the decrease of the depletion region at interface between the P3HT and TiO_2 layer. To determine the charge recombination lifetime, the EIS results of the electrodes were utilized. The charge recombination lifetime (τ) is estimated from the following equation: $\tau = (2\pi f_{max})^{-1}$, where f_{max} is the maximum frequency of the middle-frequency peak [61,62]. Correspondingly, the charge recombination lifetime was calculated to be 28.3 ms, 73.9 ms and 23.37 ms for TiO_2-NTs, Ag-TiO_2-NTs and P3HT/Ag-TiO_2-NTs electrodes, respectively. The electron life time (τ) is a measure of suppression of back reaction of injected electrons with I_3^- in the electrolyte and the lower τ value implies the increase of the electron recombination rate [63]. The lower the charge recombination lifetime for P3HT/Ag-TiO_2-NTs electrode may be the result of inefficient charge transport pathways (having a high density of traps) due to aggregation of the polymer. However, the photon-generated electrons from the P3HT (P*) can be quickly separated and transferred to the conductive band (CB) of semiconductor TiO_2-NTs in the level of femtosecond, therefore the 23.37 ms can provide enough time for the carrier transport [57]. To determine the photovoltaic properties of the Ag-TiO_2-NTs and P3HT/Ag-TiO_2-NTs electrodes, the EIS measurements were measured under simulated solar light (100 mW cm^{-2}, AM 1.5 G) and for P3HT/Ag-TiO_2-NTs electrode, the capacitance (C_{eff}) and resistance (R_1) obtained from the results were summarized in Table 2. When the Nyquist curves of the Ag-TiO_2-NTs electrode recorded under absence and present of solar light (Fig. 9) were examined, no significant change in the charge transfer resistance was observed. On the other hand, P3HT/Ag-TiO_2-NTs electrode displayed a remarkable decrease in the value of charge transfer resistance under solar light. As can be seen in Fig. 9 and Table 2, for both of light and dark environments, when the potential is scanned from 0.2 V toward the negative value (−1 V), R_1 value

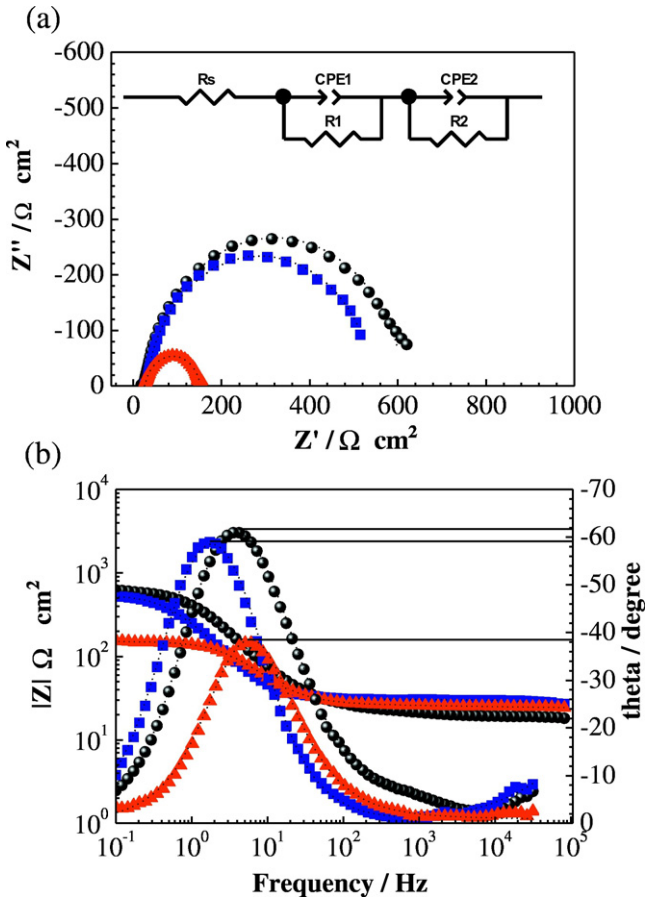


Fig. 8. Electrochemical impedance data ((a) Nyquist, (b) Bode and phase angle plots) for TiO_2-NTs (●), Ag-TiO_2-NTs (■) and P3HT/Ag-TiO_2-NTs (▲) recorded at −0.4 V in acetonitrile electrolyte contained I^-/I_3^- after 1 h of electrode immersion (fit results: ———).

Table 2
The electrical parameters obtained by fitting the experimental results of EIS for P3HT/Ag-TiO_2-NTs electrode under absence and presence of simulated sunlight illumination.

Potential (V(Ag/AgCl))	Without solar light R_1 (Ω cm^2)	Under solar light R_1 (Ω cm^2)	Without solar light C_{eff} (μF cm^{-2})	Under solar light C_{eff} (μF cm^{-2})
−1.2	25.86	14.58	4463.38	2115.59
−1.0	10.29	11.81	2102.22	2916.66
−0.8	27.84	15.42	1194.32	1766.73
−0.6	57.56	17.84	614.75	1316.44
−0.4	121.90	51.60	421.01	680.84
−0.2	7248.00	1341.00	116.83	308.06
0.2	5.19×10^8	3.11×10^4	161.76	181.29
0.4	2.09×10^6	2.56×10^4	13.66	45.93
0.6	6.53×10^4	8.58×10^3	5.96	23.57
0.8	2.39×10^4	5.19×10^3	4.46	13.70
1.0	2.51×10^4	4.34×10^3	3.20	8.97
1.2	2.99×10^4	4.96×10^3	2.82	6.97

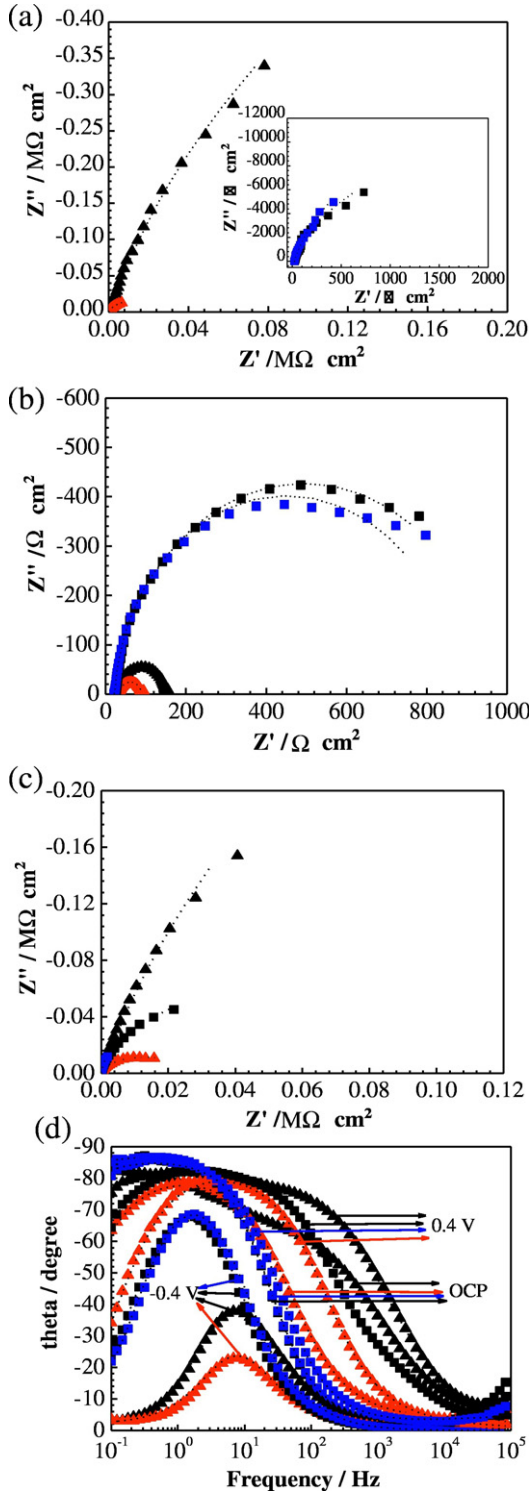


Fig. 9. Nyquist recorded at OCP (a), −0.4 V (b), 0.4 V (c) and Bode results (d) of Ag-TiO_2-NTs and P3HT/Ag-TiO_2-NTs electrodes under the absence and presence of solar light (simulated AM 1.5G (100 mW cm^{-2}) irradiance) in acetonitrile electrolyte contained I^-/I_3^- after 1 h of electrode immersion, (Ag-TiO_2-NTs (■), Ag-TiO_2-NTs in light (■), P3HT/Ag-TiO_2-NTs (▲), P3HT/Ag-TiO_2-NTs in light (▲), fit results: ———).

decreases, conversely, the capacitance (C_{eff}) value increases. The sharp decrease and increase in the resistance and capacitance values is observed at the potential range of −0.4 to −0.2. This result suggests that the bandgap trap states injected electrons are widely distributed at the negative potential of −0.2 V [64]. For higher potential values up to 0.6 V, a decrease of the resistance value is observed. This potential region describes a transition to the conducting form of the P3HT and directly characterizes the electrochemical doping of the P3HT film [65]. This potential (~0.6 V) is consistent with oxidation peaks determined from the cyclic voltammetry result (Fig. 13). For almost all potential, it is observed that the charge transfer resistance (R_1) is dramatically reduced and the capacitance value (C_{eff}) increases under the solar light, compared with the values in the absence of solar light. This can be interpreted as the increase of conductivity by photogenerated charge carriers. To investigate the photoresponse of Ag-TiO_2-NTs and P3HT/Ag-TiO_2-NTs electrodes, current-voltage characteristics were also carried out under solar light. As seen from Fig. 10, the photocurrent densities of Ag-TiO_2-NTs and P3HT/Ag-TiO_2-NTs electrodes increases with the applied potential and almost reaches a plateau-like behavior at 1.0 V for P3HT/Ag-TiO_2-NTs. The onset potential and the half wave potential shifted toward more negative potentials for P3HT/Ag-TiO_2-NTs electrode and P3HT/Ag-TiO_2-NTs electrode presents a photocurrent greater than Ag-TiO_2-NTs electrode. The negative shift shows that the charge separation and transportation in P3HT/Ag-TiO_2-NTs electrode are more efficient. Also, these results indicate that P3HT have a key role in the formation of charge carriers by solar light absorption. Open circuit potential (V_{OC})-time curves of P3HT/Ag-TiO_2-NTs electrode under absence and presence of solar light is showed in Fig. 11. In the absence of solar light, the open circuit potential of P3HT/Ag-TiO_2-NTs electrode represents the difference in the Fermi level between the P3HT/Ag-TiO_2-NTs electrode and counter electrodes, which is defined by redox equilibration. The variation in the potential upon illumination was found to be 0.15 V. The excitation of P3HT/Ag-TiO_2-NTs electrode under solar light results in charge separation, increasing the electron concentration in the active layer and causes a shift of the open circuit potential to more negative potential [66].

To determine semiconductor type, the flat band potential and charge carrier density of the TiO_2-NTs, Ag-TiO_2-NTs and P3HT/Ag-TiO_2-NTs electrodes, Mott-Schottky equation was utilized [65–68]:

$$\frac{1}{C^2} = \frac{2}{q\varepsilon\varepsilon_0 N_D}\left[(E - E_{FB}) - \frac{k_B T}{q}\right] \tag{7}$$

where C is the capacitance (F cm^{-2}), ε is the relative permittivity of the semiconductor (ε = 48 for anatase TiO_2-NTs) [69], ε_0 is the vacuum permittivity (8.854×10^{-12} F m^{-1}), q is elementary electric charge (1.602×10^{-19} C), N_D is the carrier density (cm^{-3}), E is the applied potential (V), E_{FB} is the flat band potential (V). Fig. 12a shows the Mott-Schottky (MS) plots as $1 / C^2$ vs potential for the TiO_2-NTs, Ag-TiO_2-NTs and P3HT/Ag-TiO_2-NTs electrodes. The positive slopes of MS plots

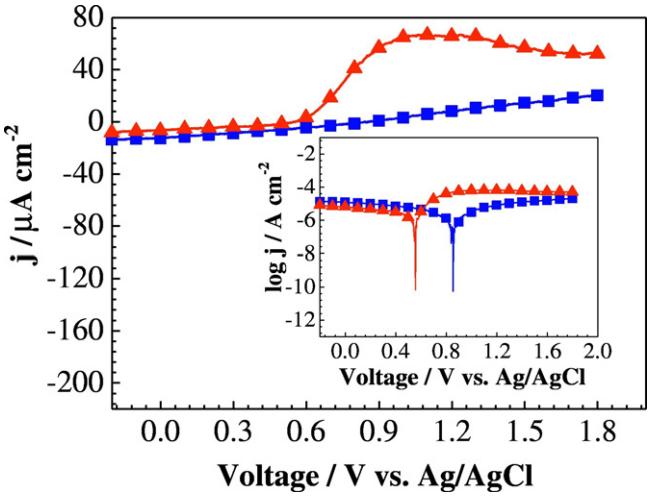


Fig. 10. Illuminated current-voltage curves of Ag-TiO_2-NTs (■) and P3HT/Ag-TiO_2-NTs (▲) electrodes after 1 h of electrode immersion in acetonitrile electrolyte contained I^-/I_3^-.

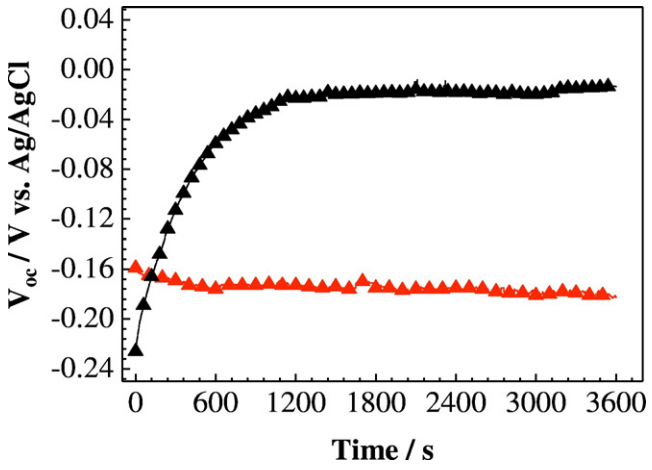


Fig. 11. Open circuit voltage-time curves of P3HT/Ag-TiO_2-NTs electrode recorded during the 1 h illuminating duration and under the absence of solar light in acetonitrile electrolyte contained I^-/I_3^-. (P3HT/Ag-TiO_2-NTs (▲), P3HT/Ag-TiO_2-NTs in light (▲)).

indicate a n-type semiconductor behavior of the obtained electrodes [67]. The carrier density (N_D) was calculated from the slope of the linear parts of curves and the flat band potential was determined by extrapolating the straight line to intersect with potential axis. The parameters obtained from MS analysis are shown in Table 3. It reveals that the Ag-doped TiO_2-NTs have a higher carrier density (N_D) than those of the other electrodes, due to the incorporation of Ag NPs in TiO_2-NTs layer make it more conductive [70]. Besides, in the literature [71,72], various metal nanoparticles (such as Au and Ag) have been incorporated into TiO_2 layer of organic solar cells for making use of the plasmonic effects to enhance the light absorption of organic solar cells. Especially silver (Ag) among noble metals exhibits a most effective optical trapping potential due to its relative stronger scattering efficiency in the visible range [73]. In these studies, it has been reported that the transferred plasmonically excited electrons from metal nanoparticles to TiO_2 can achieve trap filling in the TiO_2 layer, leading to reduce effective extraction barrier, decreased resistance and charge recombination, which can increase electron concentration in TiO_2 layer. The plasmonic effect recorded in the literature was also observed for Ag-doped TiO_2-NTs electrode. As a result, this effect provided an increase in charge carrier density of the Ag-doped TiO_2-NTs electrode. Due to the decrease of conductive depending on blocking of the centers activated with Ag NPs and the increase of electron recombination as related to the presence of defects after the coating P3HT, N_D value of P3HT/Ag-TiO_2-NTs decreases, compared to that of Ag-TiO_2-NTs. However, the increase in the N_D value for P3HT/Ag-TiO_2-NTs was observed after illumination, a situation anticipated for a photoactive film, since the creation of additional charge carriers under solar light [74]. Besides, there have been some studies reporting that the plasmonic effects of metal nanostructures improve the active layer absorption. Li et al. [73] investigated the effects of the plasmonic mixed Ag nanostructures on organic solar cell performances and reported that the incorporation of the mixed Ag nanoparticles into the absorbing layer (P3HT:PCBM film) supplies wide-band absorption improvement so that light can be best trapped inside the active layer and as a result, the mixed Ag structures device shows a high efficiency with power conversion efficiency 4.3%. In the present work, the increase in charge carrier density obtained for the P3HT/Ag-TiO_2-NTs electrode after illumination can be attributed that the plasmonic effect by the incorporated Ag nanostructures improves the electrical properties such as location of exciton generation, mobility of charge carriers, interfacial

Table 3
The carrier density N_D and the flat band potential (E_{FB}) values for TiO_2-NTs, Ag-TiO_2-NTs, P3HT/Ag-TiO_2-NTs electrodes.

	N_D (cm^{-3})	E_{FB} (V)
TiO_2-NTs	7.43×10^{21}	−0.43
Ag-TiO_2-NTs	291×10^{21}	−0.55
P3HT/Ag-TiO_2-NTs	8.69×10^{21}	−0.41
P3HT/Ag-TiO_2-NTs under solar light	70.1×10^{21}	−0.45

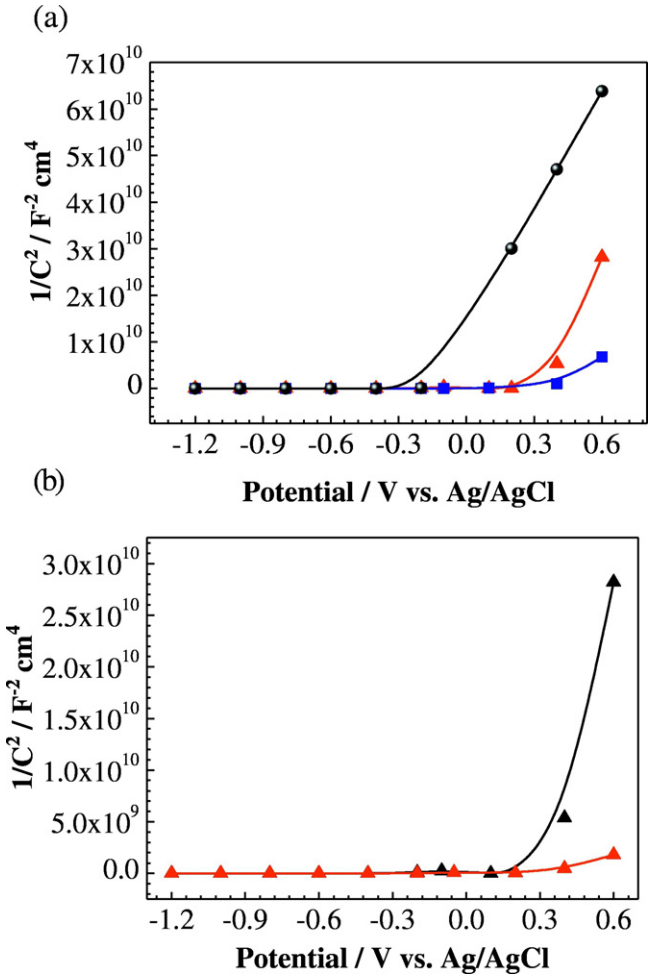


Fig. 12. Variations of $1/C^2$ with applied potential for TiO_2-NTs, Ag-TiO_2-NTs and P3HT/Ag-TiO_2-NTs electrodes under the absence of solar light (TiO_2-NTs (●), Ag-TiO_2-NTs (■) and P3HT/Ag-TiO_2-NTs (▲)), (b) Mott-Schottky plots of P3HT/Ag-TiO_2-NTs electrode obtained under presence of solar light (P3HT/Ag-TiO_2-NTs (▲), P3HT/Ag-TiO_2-NTs in light (▲)).

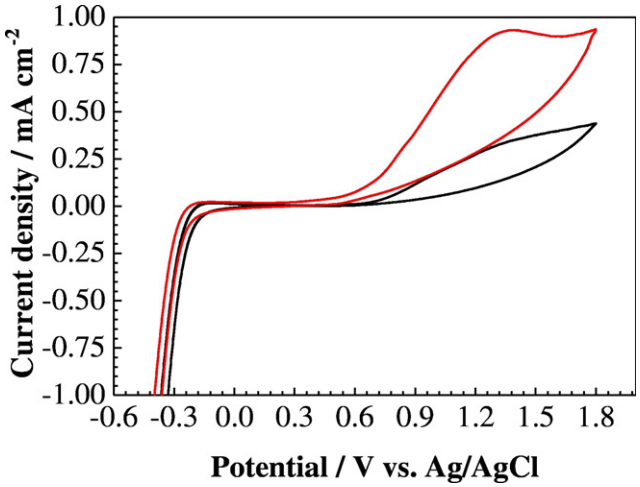


Fig. 13. Cyclic voltammetry curves of P3HT/Ag-TiO_2-NTs electrodes recorded under the absence (▬) and presence (▬) of solar light in acetonitrile electrolyte contained I^-/I_3^-.

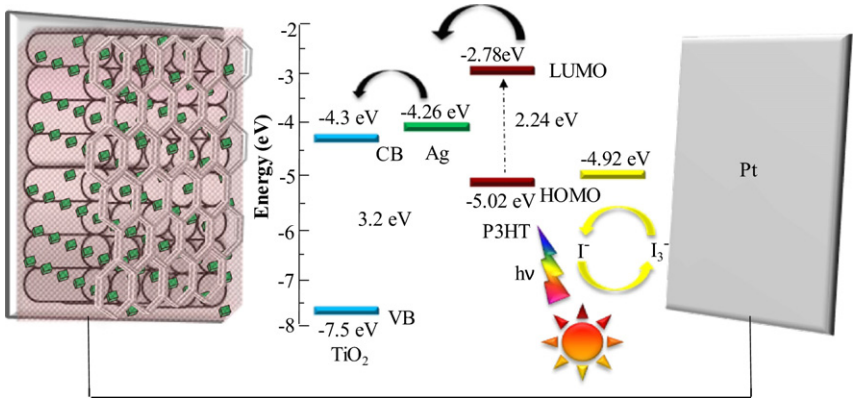


Fig. 14. Schematic energy level diagram for P3HT/Ag-TiO_2-NTs electrode.

morphologies and extraction of charge carriers in the electrode due to the generating elongated optical path and improving the light absorption in the active layer. As seen from Table 3, the significant change in the flat band potential (E_{FB}) was only observed for Ag-TiO_2-NTs. Compared to the TiO_2-NTs, the negative shift of E_{FB} could be explained by the decrease in free energy change required for the charge transfer to the conductive band of the semiconductor, thus facilitating the electron separation and transfer [69].

To investigate electronic band states of P3HT/Ag-TiO_2-NTs electrode, the CV measurements were carried out in acetonitrile electrolyte contained I^-/I_3^- at 100 mV/s under absence and presence of solar light and the results are shown in Fig. 13. When the current responses obtained at 1.4 V for P3HT/Ag-TiO_2-NTs under absence and presence of solar light are compared, P3HT/Ag-TiO_2-NTs electrode under solar light exhibits a larger integrated area and higher current response (9.31×10^{-4} A/cm^2) than that (3.52×10^{-4} A/cm^2) of P3HT/Ag-TiO_2-NTs electrode under the absence of solar light. This can be associated that the number of charge carriers increases at the P3HT-electrolyte interface after irradiation. The highest occupied molecular orbital (HOMO) was estimated from oxidation potential (E_{ox}), according to the equation of (HOMO) $= -e\,[E_{ox} + 4.4]$ and HOMO energy level of P3HT was found to be -5.02 eV. According to the energy gap (2.24 eV) of P3HT calculated from the result of Uv–Vis and the previous literatures [75,76], the schematic energy level diagram of P3HT/Ag-TiO_2-NTs is presented in Fig. 14. Under simulated solar illumination, the electrons on the HOMO of P3HT are firstly excited to the LUMO of P3HT. The excited electrons are quickly injected into Ag nanoparticles and then, transferred to the conduction band (CB) of TiO_2-NTs. At the same time, certain electrons also can be excited from valance band (VB) to CB of TiO_2-NTs because of a small part UV light of sunlight. The P3HT becomes oxidized. The oxidized P3HT* (P*) are regenerated by receiving electron from the I^- ion redox mediator that get oxidized to I_3^-. The electrolyte itself is regenerated via the platinum counter electrode by electrons passing through the external circuit. In this system, Ag NPs deposited on the TiO_2-NTs is acted as an electron sink for an efficiently electron transfer. Furthermore, the electrons constituted by the localized surface plasmon resonance in Ag NPs transfers to the CB of TiO_2-NTs and are collected by the current collector (Ti foil).

4. Conclusions

In this work, the deposition of Ag on TiO_2-NTs electrode fabricated by two-step anodization technique was performed with the galvanostatic technique. Then, the P3HT film synthesized by oxidative polymerization with $FeCl_3$ was prepared on Ag-TiO_2-NTs by spin coating technique. The characterization results of the synthesized P3HT indicated that P3HT consists of 64.7% regioregular and 35.7% regioirregular configurations and has mainly edge-on oriented lamella layer structure with a minority of face-on lamella. The measured optical band gap, the highest occupied molecular orbital (HOMO) and of P3HT were found to be 2.24 eV and -5.02 eV, respectively. The SEM images and the XRD results recorded for P3HT/Ag-TiO_2-NTs revealed that the top surface of Ag-TiO_2-NTs and the gaps between nanotubes was exactly covered by P3HT and the crystallite size of P3HT after the coating of P3HT on the Ag-TiO_2-NTs decreased, compared to pure P3HT, due to the disordering of the polymer chain. The electrochemical impedance spectroscopy (EIS) technique was employed to determine the charge transport resistance and the charge recombination lifetime. It was found that P3HT/Ag-TiO_2-NTs possesses the lower charge transfer resistance among the investigated other electrodes (Ag-TiO_2-NTs and TiO_2-NTs). When the P3HT/Ag-TiO_2-NTs system was illuminated with solar light, it was observed that the charge transfer resistance decreased and the carrier density increased as a result of the creation of additional charge carriers under solar light. The results indicate that the nanocomposite of P3HT/Ag-TiO_2-NTs has a potential for fabricating hybrid organic–inorganic solid state solar cells.

Acknowledgements

This work was financially supported by Çukurova University Scientific Research Unit (Project No : FEF2013D29) and the authors acknowledge the financial support from the Scientific and Technological Research Council of Turkey (TÜBİTAK 2211-C program).

References

[1] N. Duraisamy, N.M. Muhammad, M.T. Hyun, K.H. Choi, Structural and electrical properties of P3HT:PCBM/PEDOT:PSS thin films deposited through electrohydrodynamic atomization technique, Mater. Lett. 92 (2013) 227–230.
[2] M. Chemek, D. Khlaifia, F. Massuyeau, J.L. Duvail, E. Faulques, J. Wéry, K. Alimi, A copolymer of PVK and P3HT and its nanocomposite with single-walled carbon nanotubes, Synth. Met. 197 (2014) 246–251.
[3] Shingchung Lo, Zhike Liu, Jinhua Li, Helen Laiwa Chan, Feng Yan, Hybrid solar cells based on poly(3-hexylthiophene) and electrospun TiO_2 nanofibers modified with CdS nanoparticles, Prog. Nat. Sci. 23 (2013) 514–518.
[4] J. Bisquert, G.G. Belmonte, A. Munar, M. Sessolo, A. Soriano, H.J. Bolink, Band unpinning and photovoltaic model for P3HT:PCBM organic bulk heterojunctions under illumination, Chem. Phys. Lett. 465 (2008) 57–62.
[5] Y.Y. Yu, W.C. Chien, Y.H. Ko, C.P. Chen, C.C. Chang, Preparation of conjugated polymer-based composite thin film for application in solar cell, Thin Solid Films 584 (2015) 363–368.
[6] D.E. Motaung, G.F. Malgas, C.J. Arendse, S.E. Mavundla, C.J. Oliphant, D. Knoesen, Thermal-induced changes on the properties of spin-coated P3HT:C60 thin films for solar cell applications, Sol. Energ. Mat. Sol. C. 93 (2009) 1674–1680.
[7] Z.J. Wang, S.C. Qu, X.B. Zeng, J.P. Liu, C.S. Zhang, F.R. Tan, L. Jin, Z.G. Wang, Hybrid bulk heterojunction solar cells from a blend of poly(3-hexylthiophene) and TiO_2 nanotubes, Appl. Surf. Sci. 255 (2008) 1916–1920.
[8] J. Lee, J.Y. Jho, Fabrication of highly ordered and vertically oriented TiO_2 nanotube arrays for ordered heterojunction polymer/inorganic hybrid solar cell, Sol. Energ. Mat. Sol. C. 95 (2011) 3152–3156.
[9] D. Li, W. Sun, L. Shao, S. Wu, Z. Huang, X. Jind, Q. Zhang, Q. Li, Tailoring solar energy spectrum for efficient organic/inorganic hybrid solar cells by up-conversion luminescence nanophosphors, Electrochim. Acta 182 (2015) 416–423.
[10] M. Lu, S.M. Yang, Synthesis of poly(3-hexylthiophene) grafted TiO_2 nanotube composite, J. Colloid Interface Sci. 333 (2009) 128–134.

[11] D. Geethalakshmi, N. Muthukumarasamy, R. Balasundaraprabhu, CSA-doped PANI/TiO_2 hybrid BHJ solar cells-material synthesize and device fabrication, Mater. Sci. Semicond. Process. 51 (2016) 71–80.
[12] J. Denga, M. Wang, P. Zhang, W. Ye, Preparing ZnO nanowires in mesoporous TiO_2 photoanode by an in-situ hydrothermal growth for enhanced light-trapping in quantum dots-sensitized solar cells, Electrochim. Acta 200 (2016) 12–20.
[13] Y. Zhang, Z. Li, J. Ouyang, S.W. Tsang, J. Lu, K. Yu, J. Ding, Y. Tao, Hole transfer from PbS nanocrystal quantum dots to polymers and efficient hybrid solar cells utilizing infrared photons, Org. Electron. 13 (2012) 2773–2780.
[14] F.A. Roghabadi, K.O. Aghmiuni, V. Ahmadi, Optical and electrical simulation of hybrid solar cell based on conjugated polymer and size-tunable CdSe quantum dots: Influence of the QDs size, Org. Electron. 34 (2016) 164–171.
[15] T. Özdal, Y. Hames, E. Aslan, A comparative study on TiO_2 doped hybrid solar cells, Appl. Surf. Sci. 258 (2012) 5259–5264.
[16] L. Curkovic, D. Ljubas, S. Šegota, I. Bacic, Photocatalytic degradation of Lissamine Green B dye by using nanostructured sol–gel TiO_2 films, J. Alloys Compd. 604 (2014) 309–316.
[17] L. Dong, K. Cheng, W. Weng, C. Song, P. Du, G. Shen, G. Han, Hydrothermal growth of rutile TiO_2 nanorod films on titanium substrates, Thin Solid Films 519 (2011) 4634–4640.
[18] D. Guan, P.J. Hymel, Y. Wang, Growth mechanism and morphology control of double-layer and bamboo-type TiO_2 nanotube arrays by anodic oxidation, Electrochim. Acta 83 (2012) 420–429.
[19] S. Munir, S.M. Shah, H. Hussain, M. Siddiq, Adsorption of porphyrin and carminic acid on TiO_2 nanoparticles: a photo-active nano-hybrid material for hybrid bulk heterojunction solar cells, J. Photochem. Photobiol. B 153 (2015) 397–404.
[20] P. Zhong, X. Ma, X. Chen, R. Zhong, X. Liu, D. Ma, M. Zhang, Z. Li, Morphology-controllable polycrystalline TiO_2 nanorod arrays for efficient charge collection in dye-sensitized solar cells, Nano Energy 16 (2015) 99–111.
[21] S.Y. Ho, C. Su, S. Kathirvel, C.Y. Li, W.R. Li, Fabrication of TiO_2 nanotube-nanocube array composite electrode for dye-sensitized solar cells, Thin Solid Films 529 (2013) 123–127.
[22] D. Zhang, W.C.H. Choy, F.X. Xie, X. Li, Large-area, high-quality self-assembly electron transport layer for organic optoelectronic devices, Org. Electron. 13 (2012) 2042–2046.
[23] W.Q. Wu, B.X. Lei, H.S. Rao, Y.F. Xu, Y.F. Wang, C.Y. Su, D.B. Kuang, Hydrothermal fabrication of hierarchically anatase TiO_2 nanowire arrays on FTO glass for dye-sensitized solar cells, Sci. Rep. 3 (2013) 1352–1359.
[24] F. Xie, S.J. Cherng, S. Lu, Y.H. Chang, W.E.I. Sha, S.P. Feng, C.M. Chen, W.C.H. Choy, Functions of self-assembled ultrafine TiO_2 nanocrystals for high efficient dye-sensitized solar cells, ACS Appl. Mater. Interfaces 6 (2014) 5367–5373.
[25] B. Kılıç, N. Gedik, S. Mucur, A.S. Hergul, E. Gür, Band gap engineering and modifying surface of TiO_2 nanostructures by Fe_2O_3 for enhanced-performance of dye sensitized solar cell, Mater. Sci. Semicond. Process. 31 (2015) 363–371.
[26] C.M. Liu, C.M. Chen, Y.W. Su, S.M. Wang, K.H. Wie, The dual localized surface plasmonic effects of gold nanodots and gold nanoparticles enhance the performance of bulk heterojunction polymer solar cells, Org. Electron. 14 (2013) 2476–2483.
[27] T.S. Peretz, O. Sorias, M. Moshonov, I. Deckman, M. Orenstein, G.L. Frey, Plasmonic nanoparticle incorporation into inverted hybrid organic–inorganic solar cells, Org. Electron. 23 (2015) 144–150.
[28] S. Pillai, M.A. Green, Plasmonics for photovoltaic applications, Sol. Energ. Mat. Sol. C. 94 (2010) 1481–1486.
[29] J.V. Vaghasiya, K.K. Sonigara, K.B. Fadadu, S.S. Soni, Hybrid AgNP-TiO_2 thin film based photo anode for dye sensitized solar cell, Perspect. Sci. 8 (2016) 46–49.
[30] K. Tremel, S. Ludwigs, Morphology of P3HT in Thin Films in Relation to Optical and Electrical Properties, P3HT Revisited – From Molecular Scale to Solar Cell Devices: Sabine Ludwigs, Vol. 265 Adv. Polym. Sci. pp 39–82.
.[31] C.H. Kim, K. Kisiel, J. Jung, J. Ulanski, D. Tondelier, B. Geffroy, Y. Bonnassieux, G. Horowitz, Persistent photoexcitation effect on the poly(3-hexylthiophene) film: Impedance measurement and modeling, Synth. Met. 162 (2012) 460–465.
[32] L. Jiang, J. Zhang, W. Wang, H. Yang, F. Reisdorffer, T.P. Nguyen, Yi Dan, Optical properties of poly (3-hexylthiophene) and interfacial charge transfer between poly (3-hexylthiophene) and titanium dioxide in composites, J. Lumin. 159 (2015) 88–92.
[33] M. Lanzi, F.P. Di-Nicola, F. Errani, L. Paganin, A. Mucci, Solventless deposition of oligo- and polythiophenes for bulkheterojunction solar cells, Synth. Met. 195 (2014) 61–68.
[34] M. Rikukawa, M. Nakagawa, K. Ishida, H. Abe, K. Sanui, N. Ogata, Electrical properties of conductive Langmuir-Blodgett films comprised of head-to-tail poly (3-hexylthiophene), Thin Solid Films 284-285 (1996) 636–639.
[35] P. Costa-Bizzarria, M. Lanzi, L. Paganin, D. Caretti, F. Parenti, Poly[3-hexyl-4-(6-bromohexyl)thiophene]: a key-intermediate for the synthesis of self-plastifying multifunctional polythiophenes, Polymer 45 (2004) 8629–8637.
[36] R.D. McCullough, R.D. Lowe, M. Jayaraman, D.L. Anderson, Design, synthesis, and control of conducting polymer architectures: structurally homogeneous poly(3-alkylthiophenes), J. Organomet. Chem. 58 (1993) 904–912.
[37] N. Duraisamy, N.M. Muhammad, M.T. Hyun, K.H. Choi, Structural and electrical properties of P3HT:PCBM/PEDOT:PSS thin films deposited through electrohydro dynamic atomization technique, Mater. Lett. 92 (2013) 227–230.
[38] A. Gupta, A.J. Akhtar, S.K. Saha, In-situ growth of P3HT/graphene composites for supercapacitor application, Mater. Chem. Phys. 140 (2013) 616–621.
[39] M. Chemek, D. Khlaifia, F. Massuyeau, J.L. Duvail, E. Faulques, J. Wéry, K. Alimi, A copolymer of PVK and P3HT and its nanocomposite with single-walled carbon nanotubes, Synth. Met. 197 (2014) 246–251.
[40] J. He, Z. Su, B. Yan, L. Xiang, Y. Wang, The effects of different side groups on the properties of polythiophene, J. Macromol. Sci., Pure Appl. Chem. 44 (2007) 989–993.
[41] G. Keru, P.G. Ndungu, G.T. Mola, V.O. Nyamori, Bulk heterojunction solar cell with nitrogen-doped carbon nanotubes in the active layer: effect of nanocomposite synthesis technique on photovoltaic properties, Materials 8 (2015) 2415–2432.
[42] T.A. Skotheim, R.L. Elsenbaumer, J.R. Reynold, Handbook of Conducting Polymers, second ed. Marcel Dekker, New York, 1998.
[43] D.M. Stevens, Y. Qin, M.A. Hillmyer, C.D. Frisbie, Enhancement of the morphology and open circuit voltage in bilayer polymer/fullerene solar cells, J. Phys. Chem. C 113 (2009) 11408–11415.
[44] Q. Sun, K. Park, L. Dai, Liquid crystalline polymers for efficient bilayer bulk-heterojunction solar cells, J. Phys. Chem. C 113 (2009) 7892–7897.
[45] D. Lee, D.J. Jang, Charge-carrier relaxation dynamics of poly(3-hexylthiophene)-coated gold hybrid nanoparticles, Polymer 55 (2014) 5469–5476.
[46] F. Xing, Z. Su-Ling, C. Yu, Z. Jie, Y. Qian-Qian, G. Wei, Y. Meng-Yao, X. Zheng, X. Xu-Rong, Nano structure evolution in P3HT:PC61BM blend films due to the effects of thermal annealing or by adding solvent, Chin. Phys. B 24 (2015) 078401.
[47] Y.D. Han, S. Jeon, S.D. Kim, J.H. Kim, S.Y. Kim, J. Kim, K.S. Lee, J. Joo, Nanoscale photovoltaic characteristics of single quantum dot hybridized with poly(3-hexylthiophene), Org. Electron. 15 (2014) 2893–2902.
[48] R. Bkakri, N. Chehata, A. Ltaief, O.E. Kusmartseva, F.V. Kusmartsev, M. Song, A. Bouazizi, Effects of the graphene content on the conversion efficiency of P3HT: graphene based organic solar cells, J. Phys. Chem. Solids 85 (2015) 206–211.
[49] F. Alam, N. Kumar, V. Dutta, Study of surfactant-free lead sulfide nanocrystals-P3HT hybrid polymer solar cells, Org. Electron. 22 (2015) 44–50.
[50] R. Wang, Y. Xu, C. Wang, H. Zhao, R. Wang, X. Liao, L. Chen, G. Chen, Fabrication of ITO-rGO/Ag-NPs nanocomposite by two-step chronoamperometry electrodeposition and its characterization as SERS substrate, Appl. Surf. Sci. 349 (2015) 805–810.
[51] A.J. Leenheer, A. Miedaner, C.J. Curtis, M.F.A.M. Hest, D.S. Ginley, Fabrication of nanoporous titania on glass and transparent conducting oxide substrates by anodization of titanium films, J. Mater. Res. 22 (2007) 681–687.
[52] W. Zhu, X. Liu, H. Liu, D. Tong, J. Yang, J. Peng, An efficient approach to control the morphology and the adhesion properties of anodized TiO_2 nanotube arrays for improved photoconversion efficiency, Electrochim. Acta 56 (2011) 2618–2626.
[53] G. Li, X. Zhu, X. Tang, W. Song, Z. Yang, J. Dai, Y. Sun, X. Pan, S. Dai, Doping and annealing effects on ZnO:Cd thin films by sol–gel method, J. Alloys Compd. 509 (2011) 4816–4823.
[54] L. Zhao, M. Xia, Y. Liu, B. Zheng, Q. Jiang, J. Lian, Structure and photocatalysis of TiO_2/ZnO double-layer film prepared by pulsed laser deposition, Mater. Trans. 53 (2012) 463–468.
[55] P.G. Karagiannidis, S. Kassavetis, C. Pitsalidis, S. Logothetidis, Thermal annealing effect on the nanomechanical properties and structure of P3HT: PCBM thin films, Thin Solid Films 519 (2011) 4105–4109.
[56] Qinghua Lia, Xiao Jina, Xuwei Yanga, Changyong Chena, Zihan Chena, Yuancheng Qina, Tai-huei Weib, Weifu Sun, Reducing the excess energy offset in organic/inorganic hybrid solar cells: toward faster electron transfer, Appl. Catal. B-Environ. 162 (2015) 524–531.
[57] Y. Xiao, G. Han, Y. Chang, H. Zhou, M. Li, Y. Li, An all-solid-state perovskite-sensitized solar cell based on the dual function polyaniline as the sensitizer and p-type hole-transporting material, J. Power Sources 267 (2014) 1–8.
[58] H. Wua, D. Li, X. Zhu, C. Yang, D. Liu, X. Chen, Y. Song, L. Lu, High-performance and renewable supercapacitors based on TiO_2 nanotube array electrodes treated by an electrochemical doping approach, Electrochim. Acta 116 (2014) 129–136.
[59] B. Arredondo, B. Romero, G. Del Pozo, M. Sessler, C. Veit, U. Würfel, Impedance spectroscopy analysis of small molecule solution processed organic solar cell, Sol. Energ. Mat. Sol. C. 128 (2014) 351–356.
[60] B. Hirschorn, M.E. Orazem, B. Tribollet, V. Vivier, I. Frateur, M. Musianid, Determination of effective capacitance and film thickness from constant-phase-element parameter, Electrochim. Acta 55 (2010) 6218–6227.
[61] J. Chen, C. Li, D.W. Zhao, W. Lei, Y. Zhang, M.T. Cole, D.P. Chu, B.P. Wang, Y.P. Cui, X.W. Sun, W.I. Milne, A quantum dot sensitized solar cell based on vertically aligned carbon nanotube templated ZnO arrays, Electrochem. Commun. 12 (2010) 1432–1435.
[62] B. Liu, W. Li, B. Wang, X. Li, Q. Liu, Y. Naruta, W. Zhu, Influence of different anchoring groups in indoline dyes for dye-sensitized solar cells: electron injection, impedance and charge recombination, J. Power Sources 234 (2013) 139–146.
[63] T. Guo, Y. Chen, L. Liu, Y. Cheng, X. Zhang, Q. Li, M. Wei, B. Ma, Enhanced photovoltaic performance of dye-sensitized solar cells using TiO_2-decorated ZnO nanorod arrays grown on zinc foil, J. Power Sources 201 (2012) 408–412.
[64] S.H. Kang, J.Y. Kim, Y.E. Sung, Role of surface state on the electron flow in modified TiO_2 film incorporating carbon powder for a dye-sensitized solar cell, Electrochim. Acta 52 (2007) 5242–5250.
[65] J. Gasiorowski, A.I. Mardare, N.S. Sariciftci, A.W. Hassel, Electrochemical characterization of sub-micro-gram amounts of organic semiconductors using scanning droplet cell microscopy, J. Electroanal. Chem. 691 (2013) 77–82.
[66] R.G. Freitas, M.A. Santanna, E.C. Pereira, Preparation and characterization of TiO_2 nanotube arrays in ionic liquid for water splitting, Electrochim. Acta 136 (2014) 404–411.
[67] M. BenSalah, R. Sabot, E. Triki, L. Dhouibi, Ph. Refait, M. Jeannin, Passivity of Sanicro28 (UNS N-08028) stainless steel in polluted phosphoric acid at different temperatures studied by electrochemical impedance spectroscopy and Mott–Schottky analysis, Corros. Sci. 86 (2014) 61–70.
[68] A.G. Munoz, Semiconducting properties of self-organized TiO_2 nanotubes, Electrochim. Acta 52 (2007) 4167–4176.
[69] J. Luo, Y. Ma, H. Wang, J. Chen, Preparation of polypyrrole sensitized TiO_2 nanotube arrays hybrids for efficient photoelectrochemical water splitting, Electrochim. Acta 167 (2015) 119–125.

[70] S.R. Gollu, R. Sharma, G. Srinivas, S. Kundu, D. Gupta, Incorporation of silver and gold nanostructures for performance improvement in P3HT:PCBM inverted solar cell with rGO/ZnO nanocomposite as an electron transport layer, Org. Electron. 29 (2016) 79–87.
[71] D. Zhang, W.C.H. Choy, F. Xie, W.E.I. Sha, X. Li, B. Ding, K. Zhang, F. Huang, Y. Cao, Plasmonic electrically functionalized TiO_2 for high-performance organic solar cells, Adv. Funct. Mater. 23 (2013) 4255–4261.
[72] F.X. Xie, W.C.H. Choy, W.E.I. Sha, D. Zhang, S. Zhang, X. Li, C.W. Leung, J. Hou, Enhanced charge extraction in organic solar cells through electron accumulation effects induced by metal nanoparticles, Energy Environ. Sci. 6 (2013) 3372–3379.
[73] X. Li, W.C.H. Choy, H. Lu, W.E.I. Sha, A.H.P. Ho, Efficiency enhancement of organic solar cells by using shape-dependent broadband plasmonic absorption in metallic nanoparticles, Adv. Funct. Mater. 23 (2013) 2728–2735.
[74] M.J.L. Santos, E.M. Girotto, A.F. Nogueira, Photoelectrochemical properties of poly(terthiophene) films modified with a fullerene derivative, Thin Solid Films 515 (2006) 2644–2649.
[75] J. Yamamoto, Y. Furukawa, Raman study of the interaction between regioregular poly(3-hexylthiophene) (P3HT) and transition-metal oxides MoO_3,V_2O_5, and WO_3 in polymer solar cells, Chem. Phys. Lett. 644 (2016) 267–270.
[76] H. Xia, T. Zhang, D. Wang, J. Wang, K. Liang, Composite interfacial modification in TiO_2 nanorod array/poly (3-hexylthiophene) hybrid photovoltaic devices, J. Alloys Compd. 575 (2013) 218–222.